Atmos. Chem. Phys. Discuss., https://doi.org/10.5194/acp-2017-806
Manuscript under review for journal Atmos. Chem. Phys.
Discussion started: 1 November 2017

Atmospheric Chemistry and Physics Discussions

Using different assumptions of aerosol mixing state and chemical composition to predict CCN concentrations based on filed measurement in Beijing

Jingye Ren[1], Fang Zhang[1, 2*], Yuying Wang[1], Xinxin Fan[1], Xiaoai Jin[1], Weiqi Xu[3, 4], Yele Sun[3, 4], Maureen Cribb[5], Zhanqing Li[1, 5]

[1]*State Key Laboratory of Earth Surface Processes and Resource Ecology, College of Global Change and Earth System Science, Beijing Normal University, Beijing 100875, China*

[2]*Joint Center for Global Change Studies (JCGCS), Beijing 100875, China*

[3]*State Key Laboratory of Atmospheric Boundary Layer Physics and Atmospheric Chemistry, Institute of Atmospheric Physics, Chinese Academy of Sciences, Beijing 100029, China*

[4]*University of Chinese Academy of Sciences, Beijing 100049, China*

[5]*Earth System Science Interdisciplinary Center and Department of Atmospheric and Oceanic Science, University of Maryland, College Park, Maryland, USA*

***Correspondence to:* Fang Zhang (fang.zhang@bnu.edu.cn)**

Atmos. Chem. Phys. Discuss., https://doi.org/10.5194/acp-2017-806
Manuscript under review for journal Atmos. Chem. Phys.
Discussion started: 1 November 2017

Atmospheric Chemistry and Physics Discussions

Abstract

Understanding the impacts of aerosol chemical composition and mixing state on cloud condensation nuclei (CCN) activity in polluted area is crucial for determining CCN number concentrations (N_{CCN}) accurately. In this study, we predict CCN number concentrations (N_{CCN}) by applying κ-Köhler theory under five assumed schemes of aerosol chemical composition and mixing state based on field measurement in Beijing during the winter of 2016. Our results show that the EIS scheme (with an assumption that sulfate, nitrate, and secondary organic aerosols are internally mixed and that primary organic aerosols, POA, and black carbon, BC, are externally mixed; and the chemical composition is size dependent) achieves the best closure to predict N_{CCN} with ratios of predicted-to-measured N_{CCN} ($R_{CCN\_p/m}$) of 0.90–1.12 under both clean and polluted conditions over the campaign. Also, IB scheme (with an assumption of internal mixture and bulk chemical composition for particles) shows good closure with $R_{CCN\_p/m}$ of 1.01–1.19 under clean conditions, implying that the IB assumption is sufficient for CCN prediction in continental clean regions. On polluted days, IS scheme (assuming particles with internal mixture and chemical composition is size-resolved) achieve better closure than the IB scheme due to the heterogeneity and variations in particle composition at different sizes. The improved closure achieved using EIS and IS assumptions highlights the importance of measuring size-resolved chemical composition for CCN predictions in polluted regions. N_{CCN} is significantly underestimated (with $R_{CCN\_p/m}$ of 0.6–0.8) by using the schemes of external mixture with bulk (EB) or size-resolved composition (ES), implying that the primary particles

Atmos. Chem. Phys. Discuss., https://doi.org/10.5194/acp-2017-806
Manuscript under review for journal Atmos. Chem. Phys.
Discussion started: 1 November 2017

Atmospheric Chemistry and Physics Discussions

experience rapid aging and physical mixing processes in urban area. However, our results show that the mixing state of particles plays a minor role on CCN prediction when the κ_{org} exceeds 0.1.

1 Introduction

Atmospheric aerosol particles can serve as cloud condensation nuclei (CCN) and further affect the optical and microphysical properties of clouds (Twomey, 1977; Albrecht, 1989; Charlson et al., 1992). Apart from these effects, an increase in the aerosol number concentration may suppress the precipitation of shallow clouds and promote that of deep convective clouds (Rosenfeld et al., 2008; Li et al., 2011). CCN can grow into cloud droplets at proper water supersaturation levels, so the key challenge to understand indirect aerosol effects is to quantify the CCN nucleation spectra and its spatial and temporal variations.

The ability of aerosols to act as CCN mainly depends on the particle size, chemical composition, and mixing state (McFiggans et al., 2006; Dusek et al., 2006; Ma et al., 2013). The impacts of the size distribution and chemical composition on CCN activity has been discussed in previous studies (Dusek et al., 2006, Ervens et al., 2007; Broekhuizen et al., 2006; Yum et al., 2005, 2007; Wiedensohler et al., 2009; Deng et al., 2013; Zhang et al., 2014, 2016; Kawana et al., 2016). The effect of chemical composition is represented by a hygroscopicity parameter (κ) (Petters and Kreidenweis, 2007) that is often used to predict N_{CCN} (Moore et al., 2012; Zhang et al., 2014). However, particle composition may vary from single specie to a mixture of

multiple species for a given size. Size-resolved chemical composition thus leads to a better prediction of N_{CCN} because it allows κ varying with size (Medina et al., 2007; Wang et al., 2010; Meng et al., 2014). Variations in the mixing state to CCN activation under different solubilities of organics are also important for predicting N_{CCN} (Wang et al., 2010). The assumption of internal mixtures has been demonstrated to predict N_{CCN} well (Ervens et al., 2007; Chang et al., 2007; Andreae and Rosenfeld, 2008; Gunthe et al., 2009; Rose et al., 2008; Meng et al., 2014; Zhang et al., 2014; Li et al., 2017). However, some studies have shown that detailed information about the chemical composition and the mixing state was required because of the complexity of the solubility of organics (Broekhuizen et al., 2006; Bhattu and Tripathi, 2015) and because the CCN properties of fresh and aged aerosols are different (Gunthe et al., 2011). Therefore, the impact of different assumptions made concerning the mixing state and chemical composition on accurately quantifying CCN number concentrations needs further investigation, especially in heavily polluted regions.

Beijing, a typical polluted city, frequently experiences severe haze pollution episodes (Sun et al., 2013; Guo et al., 2014; Zheng et al., 2015), particularly in winter. Several recent studies have focused on studying particle hygroscopicity (Wu et al., 2016; Wang et al., 2017), analyzing chemical compositions (Gunthe et al., 2011), and using bulk κ to predict CCN in Beijing (e.g., Liu et al., 2014). However, to our knowledge, no CCN closure test that considers not only the chemical composition but also the mixing state in such a polluted urban area has been done. In particular, the transformation of the particle mixing state may be very quick during severe pollution

conditions (Wu et al., 2016). During pollution events, the hygroscopicity of organics and the CCN nucleation efficiency are often enhanced rapidly with the aging process (Gunthe et al., 2011; Kawana et al., 2016). Therefore, the characterization and parameterization of CCN activation may be more challenging due to the impacts of organics in polluted regions (Wang et al., 2010; Meng et al., 2014; Che et al., 2016; Zhang et al., 2016).

In this study, we use size-resolved measurements of CCN activity and size-resolved chemical composition information to predict N_{CCN} using field measurement data collected in Beijing during the winter of 2016. The CCN closure study is carried out using five schemes assuming different particle mixing state and chemical composition. By classifying the data into three different periods (nighttime, noontime, and the evening rush hour), we also investigate the variations in the aerosol mixing state from fresh to relatively aged aerosols. The sensitivity of predicted N_{CCN} to the particle mixing state and organic volume fraction with the aging of organic particles is also presented in the last section of the study.

2 Measurements and data

2.1 The site

Data used here were measured from 15 November to 14 December 2016 during the Air Pollution and Human Health (APHH) field campaign at the Institute of Atmospheric Physics (IAP), Chinese Academy of Sciences (39.97^{o}N, 116.37^{o}E),

which is a typical urban site with influences from traffic and cooking emissions (Sun et al., 2015). The sampling instruments were placed in a container at ground level. An Aerodyne High-Resolution Time-of-Flight Aerosol Mass Spectrometer (HR-ToF-AMS; DeCarlo et al., 2006) was housed in a sampling room on the rooftop of a two-story building to measure size-resolved non-refractory submicron aerosols, including organics, sulfate, nitrate, ammonium, and chloride with a time resolution of ~5 min. More details about the HR-ToF-AMS and the measurement site have been described in previous studies (Sun et al., 2010; Sun et al., 2016). The other individual instruments and measurements are described in the following sections.

2.2 Instruments and data

The particle number size distribution (PNSD) was measured by a Scanning Mobility Particle Sizer (SMPS; Wang et al., 2003). The SMPS consists of a differential mobility analyzer (DMA; model 3081, TSI Inc.) and a condensation particle counter (CPC; model 3772, TSI Inc.). Measurements of the size-resolved CCN efficiency spectra were made by an integrated system of the SMPS (Wang et al., 2003) and a Droplet Measurement Technologies CCN counter (DMT-CCNc; Lance et al., 2006). The procedure to couple the SMPS and the DMT-CCNc developed by Moore et al. (2010) was followed. Atmospheric particles were collected from a sampling inlet located 1.5 m above the roof of the container and then passed through a silica gel desiccant drying tube into the SMPS, which assured that the relative humidity of the sample flow was below 30%. The sample flow exiting the DMA was divided into 0.5

lpm for the CCNc and 0.5 lpm for the CPC. To ensure that the flow between the DMA and CPC was the same, we supplied 0.5 lpm to the CPC using a filter. Before and after the field campaign, ammonium sulfate was used to calibrate the supersaturation (SS) levels of the CCNc with longitudinal temperature gradients of 2, 3, 5, 8, 10, 13, and 15 K as shown in Fig. S1 (Rose et al., 2008). Based on this calibration, the five effective SS levels were 0.12, 0.14, 0.23, 0.40, and 0.76%.

The PNSD is within the size range of 10–550 nm and the scanning time resolution is 5 min. Raw condensation nuclei (CN) data were calculated with multiple charge correction and transfer functions according to the TSI-AIM software. The CN number concentration (N_{CN}) is the total aerosol number concentration and is obtained by integrating the PNSD over a size range of 10–550 nm. The full measurement cycle of the CCNc for the five SS levels took one hour (20 min for 0.12% and 10 min for higher SS). Size-resolved CCN efficiency data were inversed with a multiple charge correction (Moore et al., 2010). The CCN number size distribution was calculated by multiplying the CCN efficiency spectrum and the particle number size distribution. The total CCN number was then calculated by integrating the size-resolved N_{CCN}. The bulk activation ratio (AR) was calculated as N_{CCN}/N_{CN}. To examine the properties of CCN activation, polluted and background conditions were classified according to the critical mass concentration of CN (50 μg m^{-3}).

The black carbon (BC) mass concentration was measured using a seven-wavelength aethalometer (AE33, Magee Scientific Corp.). Zhao et al. (2017) provides details

about this instrument and the measurements it makes. The BC size distribution was investigated using the approximately lognormal distribution and the total BC mass concentration (Wu et al., 2017).

3 Theory

3.1 Calculation of CCN concentration using κ-Köhler theory

In this study, we used the critical dry diameter (D_p) and particle number size distribution to calculate N_{CCN}. The method to derive D_p is based upon κ-Köhler theory (Petters and Kreidenweis, 2007). In κ-Köhler theory, the water vapor saturation ratio over the aqueous solution droplet S is given by:

$$S_c = \frac{D^3 - D_P^{\,3}}{D^3 - D_P^{\,3}(1-\kappa)} \exp\left(\frac{4\sigma_w M_w}{RT\rho_W D}\right), \quad (1)$$

where D is the droplet diameter, D_p is the dry diameter of the particle, M_w is the molecular weight of water, σ_w is the surface tension of pure water, ρ_w is the density of water, R is the gas constant, and T is the absolute temperature. When $\kappa > 0.1$, it can be approximately expressed as:

$$\kappa = \frac{4A^3}{27 D_p^{\,3} \ln^2 S_c}, \quad (2)$$

$$A = \frac{4\sigma_w M_w}{RT\rho_w}, \quad (3)$$

where S_c is the particle critical supersaturation. The other variables in the equations

169 are set to: T = 298.15 K, R = 8.315 J K^{-1} mol^{-1}, ρ_w = 997.1 kg m^{-3}, M_w = 0.018015 kg
170 mol^{-1}, and σ_w = 0.072 J m^{-2} (Rose et al., 2008).

171 For internally-mixed particles, κ is calculated as follows (Petters and Kreidenweis,
172 2007; Gunthe et al., 2009):

173 $$\kappa_{chem} = \sum_i \varepsilon_i \kappa_i , \quad (4)$$

174 $$\kappa_{org} = f_{POA} \cdot \kappa_{POA} + f_{SOA} \cdot \kappa_{SOA} , \quad (5)$$

175 where κ_i and ε_i are the hygroscopicity parameter and volume fraction for the
176 individual components in the mixture, f_{POA} and f_{SOA} are the primary organic aerosol
177 (POA) mass fraction and the secondary organic aerosol (SOA) mass fraction, and i is
178 the number of components in the mixture. The Aerosol Mass Spectrometer (AMS)
179 mainly measures the particle mass size distributions of SO_4^{2-}, NO_3^-, NH_4^+ and organic
180 compounds, while the Zdanovskii-Stokes-Robinson relation requires the volume
181 fractions of the particle chemical composition (Stokes and Robinson, 1966;
182 Zdanovskii, 1948). A simplified ion pairing scheme is used to calculate the mass
183 concentrations of the inorganic salts, which suggests that NH_4NO_3 and $(NH_4)_2SO_4$ are
184 the only possible salts (Gysel et al., 2007). In this study, we considered five
185 components where $\kappa_{(NH4NO3)}$ is equal to 0.67 and $\kappa_{((NH4)2SO4)}$ is equal to 0.61 (Petters
186 and Kreidenweis, 2007; Gunthe et al., 2009). The κ_{org} is estimated using the linear
187 function derived by Mei et al. (2013), namely, κ_{org} = 2.10f_{44} - 0.11 where f_{44} is the
188 oxidation level. The mean κ_{org} is equal to 0.10 in our case. Organics are considered as

Atmos. Chem. Phys. Discuss., https://doi.org/10.5194/acp-2017-806
Manuscript under review for journal Atmos. Chem. Phys.
Discussion started: 1 November 2017

being mainly composed of two parts: POA representing non-hygroscopic particles (κ = 0) and SOA representing hygroscopic particles. In our study, the average ratios of POA and SOA to organic aerosols were 0.53 and 0.47, respectively. On the basis of equation (5), $\kappa_{(SOA)}$ is assumed to be 0.2. Also, $\kappa_{(BC)}$ is assumed to be 0.

3.2 Assumptions about chemical composition and mixing state from measurements

To examine the importance of the mixing state and chemical composition on CCN activation, five assumptions are used to predict N_{CCN}. Although the assumption of internal and external mixing is two extremely simplified schemes, it allows us to understand the importance of the mixing state on predicting N_{CCN}. In addition, size independent and dependent compositions are derived from the mass concentration of the species as measured by the AMS so that the impact of chemical composition on CCN activity can be examined.

Assumption 1: internal mixture with bulk chemical composition (IB)

In this assumption, submicron aerosol particles are assumed to be uniform and internally mixed. The bulk chemical composition shows that components are independent throughout the size range.

Assumption 2: internal mixture with size-resolved chemical composition (IS)

Submicron aerosol particles are assumed to be internally mixed and to all have the identical composition. However, the size-resolved chemical composition shows that

components vary throughout the size range. The particle components at each size is derived from mass size distribution of the five species, i.e., NH_4NO_3, $(NH_4)_2SO_4$, SOA, POA, and BC. In this assumption, the critical diameter is based on its total hygroscopicity the κ is based on the equation (4).

Assumption 3: external mixture with bulk chemical composition (EB)

Based on this assumption, submicron aerosol particles are treated as an external mixture. This means that there are five types of particles, i.e., NH_4NO_3, $(NH_4)_2SO_4$, SOA, POA, and BC, and each particle consists of a single species (Textor et al., 2006; Zhang et al., 2010). The species composition is derived from bulk mass concentrations. The volume fraction of each particle type does not vary with the size range. The critical diameter of each species is based on its κ (Wang et al., 2010). The CCN of each type is calculated as the product of the particle number concentration and the volume fraction of the species (Wang et al., 2010; Moore et al., 2012). The sum of the N_{CCN} of each species is the total CCN.

Assumption 4: external mixture with size-resolved chemical composition (ES)

This assumption is the same as EB (i.e., five types of particles, NH_4NO_3, $(NH_4)_2SO_4$, SOA, POA, and BC, and each consists of a single species) and the aerosol particles are treated as externally mixed. However, the composition used is the size-resolved chemical composition. Therefore, the volume fraction of each particle type varies with the size range. We used the volume fraction at each size and the particle number size

229 distribution to get the $PNSD_i$ of each particle type *i*. The number concentration of
230 each particle type is then obtained from the step-wise integration of the $PNSD_i$ from
231 the critical diameter based on its κ and then summed to get the total N_{CCN}.

232 **Assumption 5: sulfate, nitrate, and SOA internally mixed, and POA and BC**
233 **externally mixed with size-resolved chemical composition (EIS)**

234 At each particle size, sulfate, nitrate, and SOA are treated as internally mixed, and
235 POA and BC are externally mixed and non-hygroscopic. Only the internal mixture
236 can serve as CCN. The volume fraction of the five types of particles varies throughout
237 the size range. The N_{CCN} of the internal mixture is calculated in the same way as under
238 the assumption of IS. The total N_{CCN} was obtained from the above obtained N_{CCN} and
239 the volume fraction of the internal mixture. When SS is greater than 0.14%, the total
240 fraction of the mixture excludes the fraction of the bulk BC because the BC size
241 distribution is approximately log-normal and the mean value is 213 nm (Wu et al.,
242 2017).

243 In all, the assumption EB and ES are opposite extremes compared to the assumptions
244 I-B and I-S and may be atmospherically realistic, but allow us to understand the impact
245 of mixing state on predicting N_{CCN}.

246

247 **4 Results and discussion**

248 **4.1 Diurnal variations in aerosol properties**

Diurnal variations in mean aerosol PNSD and bulk chemical composition under polluted and background conditions are shown in Fig. 1. Significant diurnal variations in aerosol properties were observed at the IAP site during the field campaign. The PNSD showed peaks in both background (Fig. 1a) and polluted (Fig. 1b) scenarios.

The peaks seen from 1700–2000 local time (LT) were likely due to heavy primary emissions. The sharp and abrupt increase in small particles with diameters < 100 nm was likely related to fresh primary emissions from cooking and traffic sources (Wang et al., 2017; Zhao et al., 2017). Figure 1c shows peaks in D_p of ~40 nm for the background case and ~60 nm for the polluted case. The significant elevated mass concentration of POA (Fig. 1d and 1e), a non-hygroscopic species, indicates that the peaks seen in the PNSDs for the background and polluted cases were likely associated with freshly emitted externally-mixed primary particles from cooking and vehicle sources.

The peaks seen from 0800–1200 LT for the background and polluted cases were likely associated with secondary formation processes. In particular, during polluted days, although the slight increase in the number concentration of small particles from 0600 LT to 1200 LT was likely due to primary emissions during the morning rush hour, the mass concentration of secondary substances (e.g., SOA and nitrate) as well as f_{44} (the oxidation level) increased rapidly and may have played a greater role in the particle size mode. On the contrary, the mass concentration of POA decreased significantly during daytime and reached a minimum at 1600 LT because of variations in the

planetary boundary layer (PBL) height. Another reason for the decrease in POA is the particle-phase reaction of hygroscopic species on those pre-existing primary particles under polluted conditions (e.g., Dzepina et al., 2009; Cross et al., 2009). This case suggests the importance of the formation of secondary aerosols during polluted days in urban areas. On clean days, the PNSD also shows peaks in the morning and noontime (0800–1200 LT) but with much lower particle number concentrations and smaller D_p (~30–40 nm, Fig. 1c) compared to the polluted case (~100 nm). The differences in peak D_p between the background and polluted cases reflect different atmospheric chemistry processes and mechanisms of aerosol formation. For the background case, the higher values seen from 0800–1200 LT were likely related to the particle nucleation process because of the relatively strong solar radiation present then. There was also a significant increase in nitrate, SOA, and f_{44} during this period (Fig. 1d). At the same time, POA rapidly decreased, suggesting the impacts from both the variation in PBL height and the secondary transformation of POA with the secondary hygroscopic species. Starting from 1600 LT, the mass concentration of non-hygroscopic species such as POA increased again and the particle number in the Aitken mode also increased rapidly. This was likely due to strong evening traffic emissions and the decline of the PBL height. The PNSD peak during nighttime (2200–0200 LT) is mainly attributed to the lowering PBL height.

On the basis of the diurnal cycles of PNSD and chemical composition, three periods were selected to investigate the impact of chemical composition and mixing state on CCN prediction, namely, the nighttime period (0000–0200 LT), the noontime period

(1200–1400 LT), and the evening rush hour period (1700–2000 LT).

4.2 Cumulative Gaussian distribution function fit and parameters derived from the CCN efficiency

The activation fractions measured at the five supersaturation levels were fitted using the following two functions (Rose et al., 2008; Mei et al., 2013):

$$R_a(S) = \frac{E}{2} \cdot (1 + erf(\frac{\ln S - \ln S^*}{\sqrt{2\sigma_S^{\,2}}})), \quad (6)$$

$$f_{N_{CCN}/N_{CCN}} = a(1 + erf(\frac{D - D_a}{\sigma_a \sqrt{2}})), \quad (7)$$

where the maximum activation fraction (MAF) is equal to E or $2a$, S^* and D_a are the midpoint activation supersaturation and diameter, respectively, and σ_s and σ_a are the cumulative distribution function (CDF) standard deviations. During this field campaign, about 2580 size-resolved CCN efficiency spectra at five SS levels were measured. To illustrate the characteristics of the activation spectra, the CDF fits are shown in Fig. 2 and in Tables S1-2.

4.2.1 CCN activation curves and heterogeneity of chemical components

A gradual increase in size-resolved AR with SS suggests that particles had different hygroscopicities even at the same diameter. For large particles with D_p > 100 nm, no significant differences were observed in the CCN efficiency spectra during the three periods selected (Fig. 2a), suggesting a similar hygroscopicity for these larger

particles. For particles with D_p < 100 nm, the CCN efficiency spectrum observed during the evening rush hour period showed a much more gradual increase (with smaller slopes) in size-resolved AR than that derived for the other two periods. This is attributed to the strong influence of primary organic emissions, which consist of less hygroscopic and externally-mixed smaller organic particles (e.g., POA) mainly from cooking and traffic during the evening rush hour period. Particles with D_p < 100 nm emitted during the evening rush hour period need to have a higher critical SS to reach the same AR. However, when D_p > 100 nm, the slope of AR with respect to SS became steep and near to the ideal shape of pure ammonium sulfate. Che et al. (2016) have reported that the heterogeneous parameters of particles at ~150 nm are relatively stable. This may indicate that particles became more internally mixed through nucleation and coagulation from the Aitken mode to the accumulation mode.

The heterogeneity of particle chemical composition can be represented by the ratio of σ_a and D_a (i.e., σ_a/D_a), where σ_a is the fitting standard deviation derived from the cumulative Gaussian distribution function (Eqn. 7) and D_a is the critical activation diameter (Rose et al., 2010). The ratio σ_a/D_a during the three periods is shown in Fig. 2b. In general, σ_a/D_a decreased with increasing particle diameter, suggesting that the larger particles were more homogeneous. The σ_a/D_a from 1700–2000 LT was always greater than that in the other two periods, suggesting that particles during the rush hour period were more externally mixed and heterogeneous due to the influence of traffic and cooking emissions. The values of σ_a/D_a became relatively stable when the diameter exceeded 150 nm, which may indicate that particles in the accumulation

mode were mostly internally mixed.

4.2.2 Mean critical activation diameter

The critical activation diameter at different SS levels under background and polluted conditions is shown in Fig. 3. The difference in critical diameter between polluted and background cases is calculated as D_p_POL - D_p_BG. Due to the coating process, the absolute value of the difference ranged from 4.49 nm to 1.49 nm. Typically, the activation diameter increases as SS decreases, as shown in Fig. 3. But we are more concerned with the difference between the critical diameter under polluted and background conditions. From Fig. 3, at higher SS levels, the critical diameters for polluted cases were smaller than those observed on clean days. This is because particles in the accumulation mode during polluted days are more hygroscopic than those on clear days in urban Beijing according to HTDMA measurements (Wang et al., 2017). At lower SS, the critical diameter on polluted days was larger than that obtained under clean conditions, suggesting that particles with D_p of ~40 nm were more difficult to activate under polluted conditions. This is likely because during polluted days, small particles in the Aitken mode are mainly composed of POA that have a wide range of hygroscopicities. On clean days, the large amount of small particles in the Aitken mode likely arises from the atmospheric photochemistry nucleation process, which would enhance particle hygroscopicity and CCN activity. This was also observed by Wang et al., (2017) who showed that 40-nm particles present on polluted days are less hygroscopic than those present on clean days.

4.2.3 MAF

The MAF as a function of SS during the three periods under background and polluted conditions are shown in Fig. 4. Based on the calibration of the SS levels, the MAF of pure $(NH_4)_2SO_4$ particles at the different SS levels (equal to one) is also plotted. MAFs on clean and polluted days during the campaign were less than 1, which suggests that most of the particles were externally mixed (Gunthe et al., 2011). For example, the MAF for particles with D_p of ~180 nm was around 0.78 at SS = 0.12% under background conditions, indicating that ~22% of the aerosol particles could not serve as CCN. MAFs under polluted conditions were higher than those obtained under background conditions during all periods. This may be because the particles were more aged and thus more homogenous and internally mixed under polluted conditions (Wu et al., 2016; Wang et al., 2017). As expected, the MAF during 1200–1400 LT (black solid line in Fig. 4) had the highest values, which was likely due to strong photochemical reactions that would enhance the oxidation and aging levels of particles, hence favor the physiochemical mixing process.

4.3 CCN closure study and the sensitivity of predicted N_{CCN} to assumed aerosol mixing state and chemical composition

Figure 5 shows the comparisons between predicted N_{CCN} and measured N_{CCN} at different SS levels under background and polluted conditions. The ratio of predicted-to-measured N_{CCN} ($R_{CCN\_p/m}$) ranged from 0.60 to 1.16, suggesting a

significant impact of the different assumptions on CCN prediction. The EIS assumption scheme predicts N_{CCN} very well, with $R_{CCN\_p/m}$ of 0.94–0.98. For the EIS scheme, hydrophobic POA and BC are assumed to be externally mixed while the other hygroscopic species (sulfate, nitrate, and SOA) are assumed to be internal mixtures, which are physically sound (Wang et al., 2010). The result implies that the EIS represents well the actual mixing and compositions of the particles. The IS and IB schemes that assume internally-mixed particles also predict N_{CCN} well, especially when the size-resolved chemical composition is used. On background days, the prediction is improved when using the IB scheme, suggesting the homogenous composition of aerosols in clean conditions. As SS decreased, this overestimation was less pronounced. This was likely due to the limitation of the AMS measurements. The bulk composition measured by the ACSM and the AMS shows that particles had diameters near ~100–400 nm, which lead to an underestimation of the critical diameter and thus result in the overestimation of N_{CCN} at high SS. As the SS decreased, the critical diameter increased and the deviation using the IB scheme decreased at low SS. Detailed explanations about this have been given by Wang et al. (2010) and Zhang et al. (2017). Overall, the IB and IS schemes achieve CCN closure within an acceptable uncertainty of $\pm$20%. The EB and ES schemes underestimated N_{CCN} with $R_{CCN\_p/m}$ of 0.6-0.84.

To investigate the performance of the five schemes at different times of the day, the diurnal variations in the $R_{CCN\_p/m}$ (SS = 0.23%) derived by the schemes are shown in Fig. 6. In general, the IB, IS, and EIS schemes can predict N_{CCN} very well during

all periods of the day under polluted or background conditions. $R_{CCN\_p/m}$ (0.8–1.2) are within the ±20% uncertainty range. Compared with other periods, the predicted N_{CCN} during the evening rush hour period showed the most sensitivity to the different assumption schemes, especially on clean days (Fig. 6). For example, the $R_{CCN\_p/m}$ derived using the IS and EIS schemes increased from around 1.0 (at 1700 LT) to ~1.4 (at 2000 LT), and the $R_{CCN\_p/m}$ obtained using the EB scheme decreased to a minimum value of ~0.5.

These results imply that when using either the IS or EIS assumption for the evening rush hour period, N_{CCN} is overestimated by ~20–40%. This may be because that most freshly emitted POA and BC particles are hydrophobic and do not contribute to the N_{CCN} during evening traffic hours. But the IS assumption allows POA and other hydrophobic species to serve as CCN and thus leads to an overestimation of N_{CCN}. But N_{CCN} was significantly underestimated by 50% during the evening rush hour period when applying the EB scheme. The ES scheme predicted N_{CCN} better than the EB scheme from 1700–2000 LT, suggesting variations in the heterogeneous composition of the particles at different sizes. From 1300–1600 LT, N_{CCN} was slightly underestimated by the IB, IS, and EIS schemes. This underestimation might be linked to coating and aging effects due to the strong atmospheric photochemical process that occurs around noontime on clear days (Wang et al., 2010; Ma et al., 2013; Zhang et al., 2017). Under background conditions, the IB scheme achieved the best CCN closure at any time of the day, implying that the IB assumption is likely sufficient to predict CCN in clean continental regions. However, in polluted regions, the EIS and IS

417 schemes may achieve better closure.

418 When the EB or ES assumption was used for the polluted case, the predicted N_{CCN}
419 was underestimated by ~40% at night (0000–0600 LT). Expectedly, the prediction
420 using the EB and ES schemes improved during the day on polluted days, e.g., the
421 $R_{CCN\_p/m}$ changed from about 0.6 to 0.8 using the EB scheme. This is likely associated
422 with heavy urban traffic emissions during the daytime rush hour that lead to more
423 externally-mixed particles under polluted conditions. Wang et al. (2017) showed that
424 the probability density function of κ during the morning rush hour on polluted days
425 has a bimodal distribution and a hydrophobic mode from locally-impacted particles.
426 Therefore, in this case, the EB or ES assumption is similar to actual ambient
427 conditions and hence achieves better closure results. Our results also show that
428 freshly-emitted particles may experience a quick conversion and mixing with
429 pre-existing secondary particles at night on polluted days, e.g. converting from
430 externally mixed to internally mixed (or from hydrophobic to hydrophilic, along with
431 a decrease in the volume of POA and BC) as reported previously (Riemer et al., 2004;
432 Aggarwal and Kawamura, 2009; Jimenez et al., 2009; Wu et al., 2016).

433 In summary, the importance of the mixing state and chemical composition to predict
434 N_{CCN} was examined using five different assumptions for different periods of the day.
435 Our results show that the EIS assumption can predict N_{CCN} well under both
436 background and polluted conditions. Under background conditions, the internal
437 mixture with bulk chemical composition (IB) scheme achieves the best CCN closure

during all periods of the day, implying that the IB assumption is likely sufficient to predict CCN in clean continental regions. However, in polluted regions, the EIS and IS schemes may achieve better closure than the IB scheme. The ES and EB schemes generally underestimate CCN on polluted and clean days, although the EB scheme does show better estimates of daytime N_{CCN} on polluted days.

4.4 Impact of mixing state and organics volume fraction on predicted N_{CCN} and its variation with aerosol aging

To further examine the sensitivity of predicted N_{CCN} to the particle mixing state and organic volume fraction with the aging of organic particles, the relative deviation between N_{CCN} predicted using assumptions of internal and external mixtures as a function of κ_{org} is shown in Fig. 7. The schemes that assume internal and external mixtures use bulk mixtures of organics, sulfate, and nitrate, which simplifies the problem. The hygroscopicity of organics increases as they age. Assumptions made about the volume fraction and κ_{org} depend on the probability distribution functions of the two variables. During the field campaign, the volume fraction was 30, 60, and 80%, and κ_{org} varied from 0 to 0.2. The deviation between internal and external mixtures is calculated as $[(N_{CCN,}IB - N_{CCN,}EB)\ (N_{CCN,}EB)^{-1}]$. The relative deviation increased as the volume fraction of organics increased. When the volume fraction of organics was 30%, the maximum difference was less than 23% for all cases. This is consistent with previous studies that reported differences less than 20% when x_{org} < 30% (Sotiropoulou et al., 2006; Wang et al., 2010). The deviation reached 67% when

x_{org} increased to 80% at SS = 0.76%. The deviation is greatest when organics are non-hygroscopic, i.e., when κ_{org} = 0. The deviation decreased rapidly when the oxidation grew to 0.05 in all cases. When κ_{org} reached 0.1, differences were less than 20% even at low SS. Moreover, differences were 10% or less at larger SS levels. This suggests that the mixing state of particles plays a minor role when κ_{org} exceeds 0.1. The κ values of sulfate, nitrate, and SOA are always larger than 0.1, so the impact of the mixing state on predicted N_{CCN} cannot be ignored for larger fractions of POA and BC.

5 Conclusions

In this study, we have investigated the importance of aerosol chemical composition and mixing state on CCN activity based on measurements made during a field campaign carried out in Beijing in the winter of 2016. The predicted N_{CCN} was derived by applying κ-Köhler theory and using five schemes that assume different mixing state and chemical composition combinations.

A significant impact of the mixing state on CCN prediction was found. The $R_{CCN\_p/m}$ ranged from 0.60 to 1.16. The best estimates of N_{CCN} under both background and polluted conditions were obtained when using the EIS scheme with $R_{CCN\_p/m}$ of 0.90–1.12. Under background conditions, the IB scheme also provided reasonable estimates with $R_{CCN\_p/m}$ of ranging from 1.01–1.19. This implies that the IB assumption is likely sufficient to predict CCN in clean continental regions. On polluted days, the EIS and IS schemes appear to achieve better closure than the IB

480 scheme due to the heterogeneity in particle composition across different sizes. The
481 improved closure obtained using the EIS and IS assumptions suggests the importance
482 of knowing the size-resolved chemical composition for CCN prediction in polluted
483 regions. The ES and EB schemes markedly underestimate N_{CCN} on both polluted and
484 clean days with $R_{CCN\_p/m}$ of 0.6–0.8. The EB scheme showed a significant
485 improvement in predicting daytime N_{CCN} on polluted days. The diurnal variations in
486 the $R_{CCN\_p/m}$ show that the predicted N_{CCN} during the evening rush hour period shows
487 most sensitive to the mixing state assumptions. The $R_{CCN\_p/m}$ ranged from ~0.5 to ~1.4,
488 reflecting the impact from evening traffic and cooking sources (both with large
489 amounts of hydrophobic POA).

490 We finally examined the sensitivity of predicted N_{CCN} to the particle mixing state
491 and organic volume fraction with the aging of organic particles. Our results suggest
492 that the mixing state of particles plays a minor role when κ_{org} exceeds 0.1. However,
493 the deviation reached 67% when x_{org} increased to 80% at SS = 0.76% and κ_{org} = 0,
494 implying that the mixing state on predicted N_{CCN} cannot be ignored when there is a
495 larger fraction of organics.

496

497 **Acknowledgements.** This work was funded by the NSFC research project (41675141
498 and 91544217), the fundamental Research Funds for the Central Universities, the
499 National Basic Research Program of China '973' (2013CB955800), the NSCF-TAMU
500 Collaborative Research Grant Program (4141101031), and the Natural Science

501 Foundation (NSF) (AGS1534670). We thank all participants of the field campaign for
502 their tireless work and cooperation.

503

References

Aggarwal, S. G., and Kawamura, K.: Carbonaceous and inorganic composition in long-range transported aerosols over northern Japan: Implication for aging of water-soluble organic fraction, Atmos. Environ., 43, 2532–2540, doi:10.1016/j.atmosenv.2009.02.032, 2009.

Albrecht, B. A.: Aerosols, cloud microphysics, and fractional cloudiness, Science, 245, 1227–1230, 1989.

Andreae, M. O., and Rosenfeld, D.: Aerosol–cloud–precipitation interactions. Part 1. The nature and sources of cloud-active aerosols, Earth-Science Reviews, 89, 13–41, doi:10.1016/j.earscirev.2008.03.001, 2008.

Bhattu, D., and Tripathi, S. N.: CCN closure study: Effects of aerosol chemical composition and mixing state, J. Geophys. Res. Atmos., 120, 766–783, doi:10.1002/2014jd021978, 2015.

Broekhuizen, K., Chang, R. Y. W., Leaitch, W. R., Li, S. M., and Abbatt, J. P. D.: Closure between measured and modeled cloud condensation nuclei (CCN) using size-resolved aerosol compositions in downtown Toronto, Atmos. Chem. Phys., 6, 2513–2524, 10.5194/acp-6-2513-2006, 2006.

Chang, R. Y. W., Liu, P. S. K., Leaitch, W. R., and Abbatt, J. P. D.: Comparison between measured and predicted CCN concentrations at Egbert, Ontario: Focus on the organic aerosol fraction at a semirural site, Atmos. Environ., 41, 8172–8182, 2007.

Charlson, R. J., Schwartz, S. E., Hales, J. M., Cess, R. D., Coakley, J. A., Jr., Hansen, J. E., and Hofmann, D. J.: Climate forcing by anthropogenic aerosols, Science, 255, 423+, 1992.

Che, H. C., Zhang, X. Y., Wang, Y. Q., Zhang, L., Shen, X. J., Zhang, Y. M., Ma, Q. L., Sun, J. Y., Zhang, Y. W., and Wang, T. T.: Characterization and parameterization of aerosol cloud condensation nuclei activation under different pollution conditions, Sci. Rep, 6, doi:10.1038/srep24497, 2016.

Cross, E. S., Onasch, T. B., Canagaratna, M., Jayne, J. T., Kimmel, J., Yu, X. Y., Alexander, M. L., Worsnop, D. R., and Davidovits, P.: Single particle characterization using a light scattering module coupled to a time of flight aerosol mass spectrometer, Atmos. Chem. Phys., 9, 7769–7793, doi:10.5194/acp-9-7769-2009, 2009.

Dall'Osto, M., Harrison, R. M., Coe, H., Williams, P. I., and Allan, J. D.: Real time chemical characterization of local and regional nitrate aerosols, Atmos. Chem. Phys., 9, 3709–3720, 10.5194/acp-9-3709-2009, 2009.

DeCarlo, P. F., Kimmel, J. R., Trimborn, A., et al.: Field-deployable, high-resolution,

536 time-of-flight aerosol mass spectrometer, Anal. Chem., 78, 8281–8289, 2006.

537 Deng, Z. Z., Zhao, C. S., Ma, N., Ran, L., Zhou, G. Q., Lu, D. R., and Zhou, X. J.: An examination
538 of parameterizations for the CCN number concentration based on in situ measurements of
539 aerosol activation properties in the North China Plain, Atmos. Chem. Phys., 13, 6227–6237,
540 10.5194/acp-13-6227-2013, 2013.

541 Dusek, U., Frank, G. P., Hildebrandt, L., et al.: Size matters more than chemistry for cloud
542 nucleating ability of aerosol particles, Science, 312, 1375–1378, 2006.

543 Dzepina, K., Volkamer, R. M., Madronich, S., Tulet, P., Ulbrich, I. M., Zhang, Q., Cappa, C. D.,
544 Ziemann, P. J., and Jimenez, J. L.: Evaluation of recently proposed secondary organic aerosol
545 models for a case study in Mexico City, Atmos. Chem. Phys., 9, 5681–5709,
546 doi:10.5194/acp-9-5681-2009, 2009.

547 Ervens, B., Cubison, M., Andrews, E., et al.: Prediction of cloud condensation nucleus number
548 concentration using measurements of aerosol size distributions and composition and light
549 scattering enhancement due to humidity, J. Geophys. Res. Atmos., 112, D10S32,
550 doi:10.1029/2006JD007426, 2007.

551 Gunthe, S. S., King, S. M., Rose, D., Chen, Q., Roldin, P., Farmer, D. K., Jimenez, J. L., Artaxo, P.,
552 Andreae, M. O., Martin, S. T., and Pöschl, U.: Cloud condensation nuclei in pristine tropical
553 rainforest air of Amazonia: size resolved measurements and modeling of atmospheric aerosol
554 composition and CCN activity, Atmos. Chem. Phys., 9, 7551–7575,
555 doi:10.5194/acp-9-7551-2009, 2009.

556 Gunthe, S. S., Rose, D., Su, H., Garland, R. M., Achtert, P., Nowak, A., Wiedensohler, A., Kuwata,
557 M., Takegawa, N., Kondo, Y., Hu, M., Shao, M., Zhu, T., Andreae, M. O., and Pöschl, U.: Cloud
558 condensation nuclei (CCN) from fresh and aged air pollution in the megacity region of Beijing,
559 Atmos. Chem. Phys., 11, 11023–11039, doi:10.5194/acp-11-11023-2011, 2011.

560 Guo, S., Hu, M., Zamora, M. L., Peng, J., Shang, D., Zheng, J., Du, Z.,Wu, Z., Shao, M., Zeng, L.,
561 Molina, M. J., and Zhang, R.: Elucidating severe urban haze formation in China, P. Natl. Acad.
562 Sci. USA, 111, 17373–17378, doi:10.1073/pnas.1419604111, 2014.

563 Gysel, M., Crosier, J., Topping, D. O., Whitehead, J. D., Bower, K. N., Cubison, M. J., Williams, P.
564 I., Flynn, M. J., McFiggans, G. B., and Coe, H.: Closure study between chemical composition
565 and hygroscopic growth of aerosol particles during TORCH2, Atmos. Chem. Phys., 7, 6131–
566 6144, doi:10.5194/acp-7-6131-2007, 2007.

567 Jimenez, J. L., Canagaratna, M. R., et al.: Evolution of organic aerosols in the atmosphere,
568 Science, 326, 1525–1529, 2009.

569 Kawana, K., Nakayama, T., and Mochida, M.: Hygroscopicity and CCN activity of atmospheric
570 aerosol particles and their relation to organics: Characteristics of urban aerosols in Nagoya,
571 Japan, J. Geophys. Res. Atmos., 121, 4100–4121, doi:10.1002/2015jd023213, 2016.

572 Lance, S., Medina, J., Smith, J., and Nenes, A.: Mapping the operation of the DMT continuous
573 flow CCN counter, Aerosol Sci. Technol., 40, 242–254, 2006.

574 Li, Y., Zhang, F., Li, Z., Sun, L., Wang, Z., Li, P., Sun, Y., Ren, J., Wang, Y., Cribb, M., and Yuan,
575 C.: Influences of aerosol physiochemical properties and new particle formation on CCN activity
576 from observation at a suburban site of China, Atmos. Res., 188, 80–89,
577 doi:10.1016/j.atmosres.2017.01.009, 2017.

578 Li, Z., F. Niu, J. Fan, Y. Liu, D. Rosenfeld, and Y. Ding.: The long-term impacts of aerosols on the
579 vertical development of clouds and precipitation, Nature Geosci. 4, doi: 10.1038/NGEO1313,
580 2011.

581 Liu, H. J., Zhao, C. S., Nekat, B., Ma, N., Wiedensohler, A., van Pinxteren, D., Spindler, G.,
582 Müller, K., and Herrmann, H.: Aerosol hygroscopicity derived from size-segregated chemical
583 composition and its parameterization in the North China Plain, Atmos. Chem. Phys., 14, 2525–
584 2539, doi:10.5194/acp-14-2525-2014, 2014.

585 Ma, Y., Brooks, S. D., Vidaurre, G., Khalizov, A. F., Wang, L., and Zhang, R..: Rapid modification
586 of cloud-nucleating ability of aerosols by biogenic emissions, Geophys. Res. Lett., 40(23),
587 6293–6297, 2013.

588 McFiggans, G., Artaxo, P., Baltensperger, U., Coe, H., Facchini, M. C., Feingold, G., Fuzzi, S.,
589 Gysel, M., Laaksonen, A., Lohmann, U., Mentel, T. F., Murphy, D. M., O'Dowd, C. D., Snider,
590 J. R., and Weingartner, E.: The effect of physical and chemical aerosol properties on warm
591 cloud droplet activation, Atmos. Chem. Phys., 6, 2593–2649, doi:10.5194/acp-6-2593-2006,
592 2006.

593 Medina, J., Nenes, A., Sotiropoulou, R. E. P., Cottrell, L. D., Ziemba, L. D., Beckman, P. J., and
594 Griffin, R. J.: Cloud condensation nuclei closure during the International Consortium for
595 Atmospheric Research on Transport and Transformation 2004 campaign: Effects of size
596 resolved composition, J. Geophys. Res. Atmos., 112, D10S31, doi:10.1029/2006JD007588,
597 2007.

598 Mei, F., Setyan, A., Zhang, Q., and Wang, J.: CCN activity of organic aerosols observed
599 downwind of urban emissions during CARES, Atmos. Chem. Phys., 13, 12155–12169,
600 doi:10.5194/acp-13-12155-2013, 2013.

601 Meng, J. W., Yeung, M. C., Li, Y. J., Lee, B. Y. L., and Chan, C. K.: Size-resolved cloud
602 condensation nuclei (CCN) activity and closure analysis at the HKUST Supersite in Hong Kong,
603 Atmos. Chem. Phys., 14, 10267–10282, doi:10.5194/acp-14-10267-2014, 2014.

604 Moore, R. H., Nenes, A., and Medina, J.: Scanning mobility CCN analysis—A method for fast
605 measurements of size-resolved CCN distributions and activation kinetics, Aerosol Sci. Technol.,
606 44, 861–871, doi:10.1080/02786826.2010.498715, 2010.

607 Moore, R. H., Cerully, K., Bahreini, R., Brock, C. A., Middlebrook, A. M., and Nenes, A.:
608 Hygroscopicity and composition of California CCN during summer 2010, J. Geophys. Res.
609 Atmos., 117, D00V12, doi:10.1029/2011JD017352, 2012.

610 Petters, M. D., and Kreidenweis, S. M.: A single parameter representation of hygroscopic growth
611 and cloud condensation nucleus activity, Atmos. Chem. Phys., 7, 1961–1971,
612 doi:10.5194/acp-7-1961-2007, 2007.

613 Riemer, N., Vogel, H., and Vogel, B.: Soot aging time scales in polluted regions during day and
614 night, Atmos. Chem. Phys., 4, 1885–1893, doi:10.5194/acp-4-1885-2004, 2004.

615 Rose, D., Gunthe, S. S., Mikhailov, E., Frank, G. P., Dusek, U., Andreae, M. O., and Pöschl, U.:
616 Calibration and measurement uncertainties of a continuous-flow cloud condensation nuclei
617 counter (DMT-CCNC): CCN activation of ammonium sulfate and sodium chloride aerosol
618 particles in theory and experiment, Atmos. Chem. Phys., 8, 1153–1179,
619 doi:10.5194/acp-8-1153-2008, 2008.

620 Rose, D., Nowak, A., Achtert, P., Wiedensohler, A., Hu, M., Shao, M., Zhang, Y., Andreae, M. O.,
621 and Pöschl, U.: Cloud condensation nuclei in polluted air and biomass burning smoke near the
622 mega-city Guangzhou, China. Part 1: Size-resolved measurements and implications for the
623 modeling of aerosol particle hygroscopicity and CCN activity, Atmos. Chem. Phys., 10, 3365–
624 3383, doi:10.5194/acp-10-3365-2010, 2010.

625 Rosenfeld, D., Lohmann, U., Raga, G. B., O'Dowd, C. D., Kulmala, M., Fuzzi, S., Reissell, A.,
626 and Andreae, M. O.: Flood or drought: How do aerosols affect precipitation?, Science, 321,
627 doi:10.1126/science.1160606, 2008.

628 Sotiropoulou, R.-E. P., Medina, J., and Nenes, A.: CCN predictions: Is theory sufficient for
629 assessments of the indirect effect?, Geophys. Res. Lett., 33, doi:10.1029/2005gl025148, 2006.

630 Stokes, R. H., and Robinson, R. A.: Interactions in aqueous nonelectrolyte solutions. I.
631 Solute-solvent equilibria, J. Phys. Chem., 70, 2126–2130, 1966.

632 Sun, J., Zhang, Q., Canagaratna, M. R., Zhang, Y., Ng, N. L., Sun, Y., Jayne, J. T., Zhang, X.,
633 Zhang, X., and Worsnop, D. R.: Highly time- and size-resolved characterization of submicron

aerosol particles in Beijing using an Aerodyne Aerosol Mass Spectrometer, Atmos. Environ., 44, 131–140, doi:10.1016/j.atmosenv.2009.03.020, 2010.

Sun, Y. L., Wang, Z. F., Fu, P. Q., Yang, T., Jiang, Q., Dong, H. B., Li, J., and Jia, J. J.: Aerosol composition, sources and processes during wintertime in Beijing, China, Atmos. Chem. Phys., 13, 4577–4592, doi:10.5194/acp-13-4577-2013, 2013.

Sun, Y. L., Wang, Z. F., Du, W., Zhang, Q., Wang, Q. Q., Fu, P. Q., Pan, X. L., Li, J., Jayne, J., and Worsnop, D. R.: Long-term real-time measurements of aerosol particle composition in Beijing, China: Seasonal variations, meteorological effects, and source analysis, Atmos. Chem. Phys., 15, 10149–10165, doi:10.5194/acp-15-10149-2015, 2015.

Sun, Y., Chen, C., Zhang, Y., Xu, W., Zhou, L., Cheng, X., Zheng, H., Ji, D., Li, J., Tang, X., Fu, P., and Wang, Z.: Rapid formation and evolution of an extreme haze episode in Northern China during winter 2015, Sci. Rep., 6, doi:10.1038/srep27151, 2016.

Textor, C., Schulz, M., Guibert, S., Kinne, S., Balkanski, Y., Bauer, S., Berntsen, T., Berglen, T., Boucher, O., Chin, M., Dentener, F., Diehl, T., Easter, R., Feichter, H., Fillmore, D., Ghan, S., Ginoux, P., Gong, S., Grini, A., Hendricks, J., Horowitz, L., Huang, P., Isaksen, I., Iversen, I., Kloster, S., Koch, D., Kirkevåg, A., Kristjansson, J. E., Krol, M., Lauer, A., Lamarque, J. F., Liu, X., Montanaro, V., Myhre, G., Penner, J., Pitari, G., Reddy, S., Seland, Ø., Stier, P., Takemura, T., and Tie, X.: Analysis and quantification of the diversities of aerosol life cycles within AeroCom, Atmos. Chem. Phys., 6, 1777–1813, doi:10.5194/acp-6-1777-2006, 2006.

Twomey, S.: The influence of pollution on the shortwave albedo of clouds, J. Atmos. Sci., 34, 1149–1152, doi:10.1175/1520-0469(1977)034(1149: TIOPOT)2.0.CO;2, 1977.

Wang, J., Flagan, R. C., and Seinfeld, J. H.: A differential mobility analyzer (DMA) system for submicron aerosol measurements at ambient relative humidity, Aerosol Sci. Technol., 37, 46–52, 2003.

Wang, J., Cubison, M. J., Aiken, A. C., Jimenez, J. L., and Collins, D. R.: The importance of aerosol mixing state and size-resolved composition on CCN concentration and the variation of the importance with atmospheric aging of aerosols, Atmos. Chem. Phys., 10, 7267–7283, doi:10.5194/acp-10-7267-2010, 2010.

Wang, Y., Zhang, F., Li, Z., Tan, H., Xu, H., Ren, J., Zhao, J., Du, W., and Sun, Y.: Enhanced hydrophobicity and volatility of submicron aerosols under severe emission control conditions in Beijing, Atmos. Chem. Phys., 17, 5239–5251, doi:10.5194/acp-17-5239-2017, 2017.

Wiedensohler, A., Cheng, Y. F., Nowak, A., Wehner, B., Achtert, P., Berghof, M., Birmili, W., Wu, Z. J., Hu, M., Zhu, T., Takegawa, N., Kita, K., Kondo, Y., Lou, S. R., Hofzumahaus, A., Holland,

F., Wahner, A., Gunthe, S. S., Rose, D., Su, H., and Pöschl, U.: Rapid aerosol particle growth and increase of cloud condensation nucleus activity by secondary aerosol formation and condensation: A case study for regional air pollution in northeastern China, J. Geophys. Res. Atmos., 114, D00G08, doi:10.1029/2008JD010884, 2009.

Wu, Y., Wang, X., Tao, J., Huang, R., Tian, P., Cao, J., Zhang, L., Ho, K.-F., Han, Z., and Zhang, R.: Size distribution and source of black carbon aerosol in urban Beijing during winter haze episodes, Atmos. Chem. Phys., 17, 7965–7975, doi:10.5194/acp-17-7965-2017, 2017.

Wu, Z. J., Zheng, J., Shang, D. J., Du, Z. F., Wu, Y. S., Zeng, L. M., Wiedensohler, A., and Hu, M.: Particle hygroscopicity and its link to chemical composition in the urban atmosphere of Beijing, China, during summertime, Atmos. Chem. Phys., 16, 1123–1138, doi:10.5194/acp-16-1123-2016, 2016.

Yum, S. S., Hudson, J. G., Song, K. Y., and Choi, B. C.: Springtime cloud condensation nuclei concentrations on the west coast of Korea, Geophys. Res. Lett., 32, L09814, doi:10.1029/2005GL022641, 2005. :

Yum, S. S., Roberts, G., Kim, J. H., Song, K. Y., and Kim, D. Y.: Submicron aerosol size distributions and cloud condensation nuclei concentrations measured at Gosan, Korea, during the Atmospheric Brown Clouds East Asian Regional Experiment 2005, J. Geophys. Res. Atmos., 112, D22S32, doi:10.1029/2006JD008212, 2007.

Zdanovskii, B.: Novyi Metod Rascheta Rastvorimostei Elektrolitovv Mnogokomponentnykh Sistema, Zh. Fiz. Khim+, 22, 1478–1495, 1948.

Zhang, F., Li, Y., Li, Z., Sun, L., Li, R., Zhao, C., Wang, P., Sun, Y., Liu, X., Li, J., Li, P., Ren, G., and Fan, T.: Aerosol hygroscopicity and cloud condensation nuclei activity during the AC^{3}Exp campaign: Implications for cloud condensation nuclei parameterization, Atmos. Chem. Phys., 14, 13423–13437, doi:10.5194/acp-14-13423-2014, 2014.

Zhang, F., Li, Z., Li, Y., Sun, Y., Wang, Z., Li, P., Sun, L., Wang, P., Cribb, M., Zhao, C., Fan, T., Yang, X., and Wang, Q.: Impacts of organic aerosols and its oxidation level on CCN activity from measurement at a suburban site in China, Atmos. Chem. Phys., 16, 5413–5425, doi:10.5194/acp-16-5413-2016, 2016.

Zhang F., Wang Y., Peng J., Ren J., Zhang R., Sun Y., Don Collin., Yang X., Li Z.: Remarkable underestimation of CCN activity by ignoring aging/coating effect in aged atmosphere, J. Geophys. Res. Atmos., 2017, under review.

Zhang, Z., Engling, G., Lin, C.-Y., Chou, C. C. K., Lung, S.-C. C., Chang, S.-Y., Fan, S., Chan, C.-Y., and Zhang, Y.-H.: Chemical speciation, transport and contribution of biomass burning

700 smoke to ambient aerosol in Guangzhou, a mega city of China, Atmos. Environ., 44, 3187–3195,
701 doi:10.1016/j.atmosenv.2010.05.024, 2010.

702 Zhao, J., Du, W., Zhang, Y., Wang, Q., Chen, C., Xu, W., Han, T., Wang, Y., Fu, P., Wang, Z., Li,
703 Z., and Sun, Y.: Insights into aerosol chemistry during the 2015 China Victory Day parade:
704 results from simultaneous measurements at ground level and 260 m in Beijing, Atmos. Chem.
705 Phys., 17, 3215–3232, doi:10.5194/acp-17-3215-2017, 2017.

706 Zheng, G. J., Duan, F. K., Su, H., Ma, Y. L., Cheng, Y., Zheng, B., Zhang, Q., Huang, T., Kimoto,
707 T., Chang, D., Pöschl, U., Cheng, Y. F., and He, K. B.: Exploring the severe winter haze in
708 Beijing: the impact of synoptic weather, regional transport and heterogeneous reactions, Atmos.
709 Chem. Phys., 15, 2969–2983, doi:10.5194/acp-15-2969-2015, 2015.

710

711

712

713

714

715

716

717

718

719

720

721

722

Atmos. Chem. Phys. Discuss., https://doi.org/10.5194/acp-2017-806
Manuscript under review for journal Atmos. Chem. Phys.
Discussion started: 1 November 2017

723

724 **Figures**

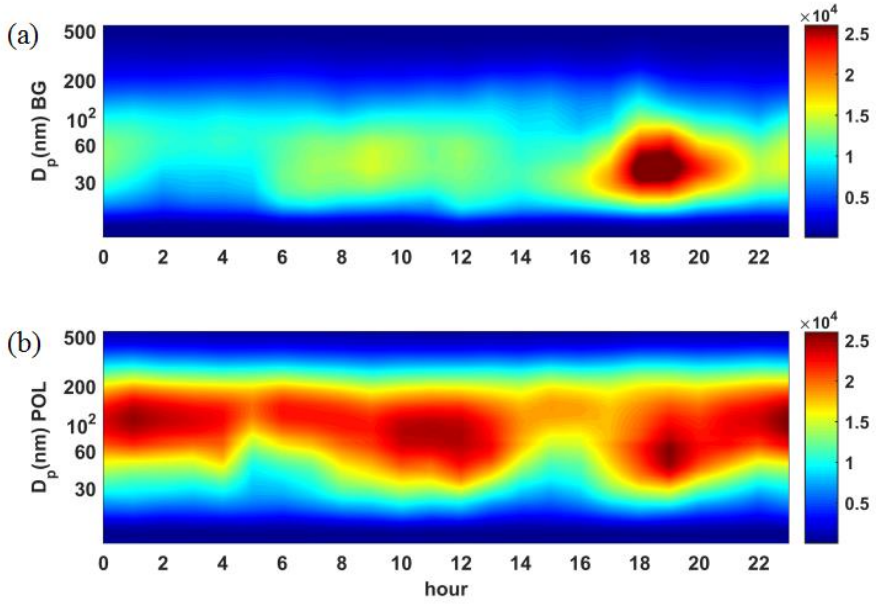

725

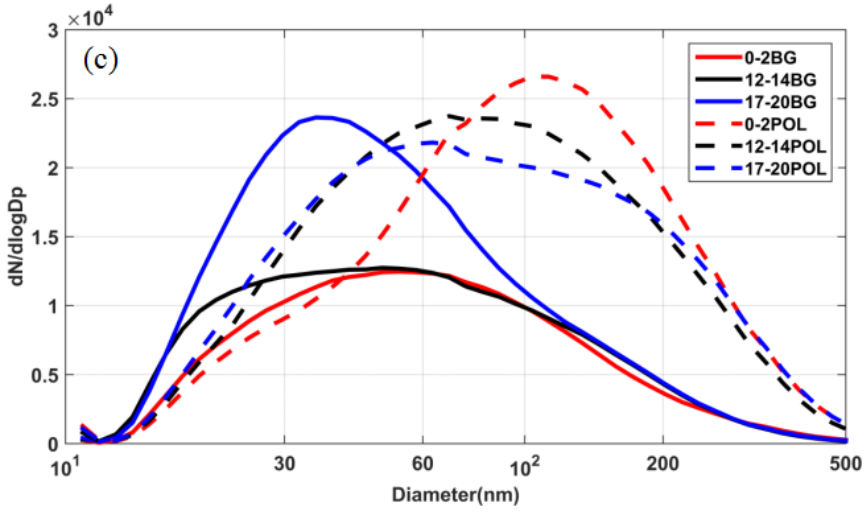

726

727

728

Atmos. Chem. Phys. Discuss., https://doi.org/10.5194/acp-2017-806
Manuscript under review for journal Atmos. Chem. Phys.
Discussion started: 1 November 2017

Atmospheric Chemistry and Physics Discussions

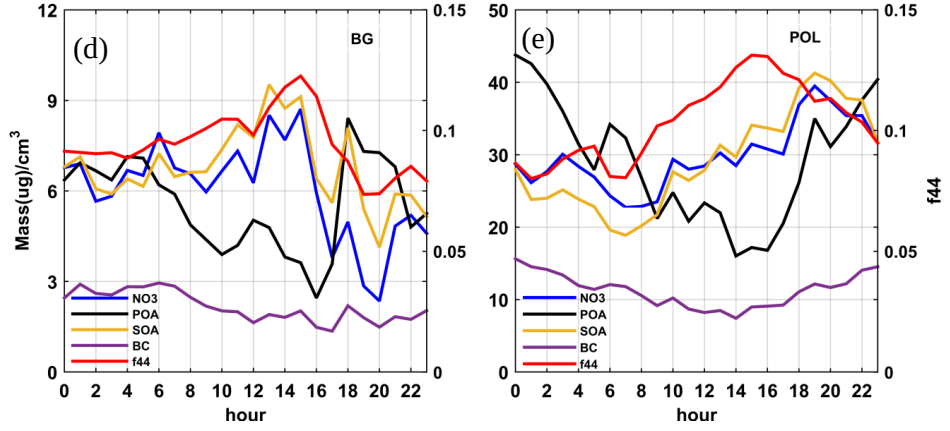

729

730 **Figure 1.** Diurnal variations in aerosol properties at the IAP site during the APHH
731 field experiment, including the particle number size distribution measured by the
732 SMPS under (a) background (BG) and (b) polluted (POL) conditions; (c) mean
733 particle number size distribution measured by the SMPS during three periods (0000–
734 0200 LT, 1200–1400 LT, and 1700–2000 LT) under BG and POL conditions; bulk
735 chemical component mass concentrations (NO_3, POA, SOA, and BC) and f_{44} derived
736 from AMS measurements made under (d) BG and (e) POL conditions.

737

Atmos. Chem. Phys. Discuss., https://doi.org/10.5194/acp-2017-806
Manuscript under review for journal Atmos. Chem. Phys.
Discussion started: 1 November 2017

Atmospheric Chemistry and Physics Discussions

738

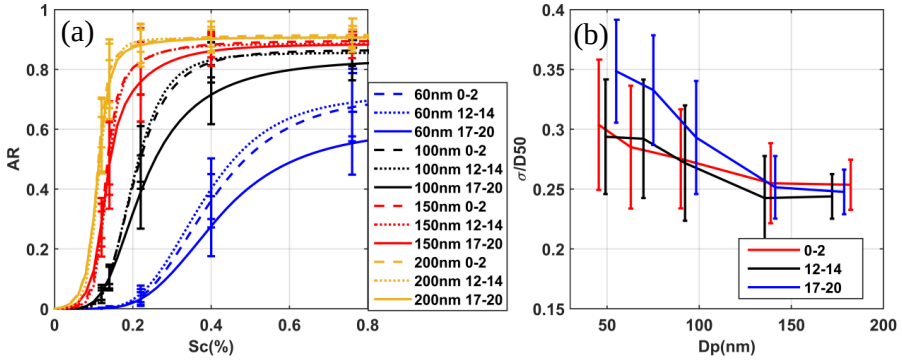

739 **Figure 2.** (a) Averaged fitted CCN efficiency spectra during the nighttime period
740 (0000–0200 LT, dashed lines), the noontime period (1200–1400 LT, dotted lines) and
741 the evening rush hour period (1700–2000 LT, solid lines) for different diameters (60,
742 100, 150, and 200 nm); (b) the heterogeneity of aerosol particles (σ_a/D_a) derived from
743 Equation (7) during the three selected periods.

744

Atmos. Chem. Phys. Discuss., https://doi.org/10.5194/acp-2017-806
Manuscript under review for journal Atmos. Chem. Phys.
Discussion started: 1 November 2017

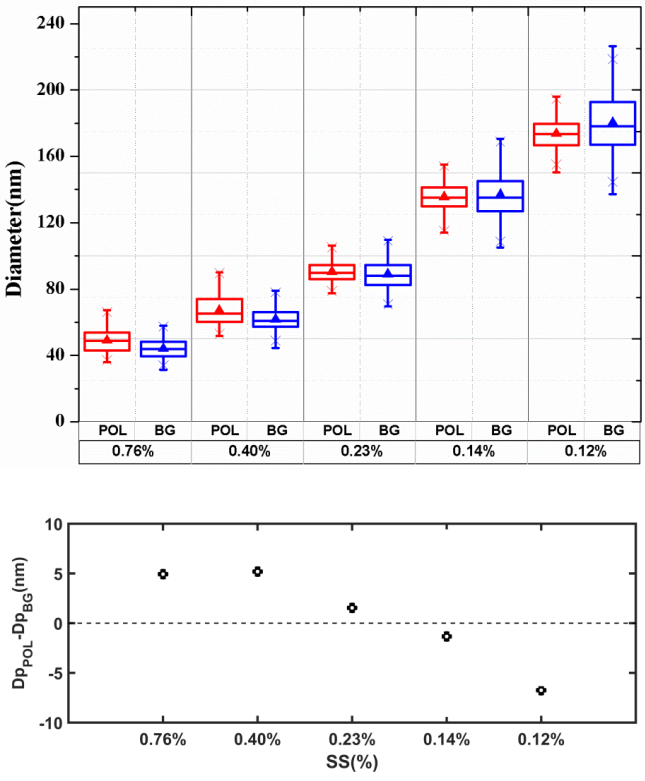

Figure 3. Top: Retrieved mean critical activation diameters at SS = 0.12, 0.14, 0.23, 0.40, and 0.76% under background (BG) and polluted (POL) conditions. The box plots show mean critical activation diameters at the 25th, 50th, and 75th percentiles. Bottom: Difference in the mean critical activation diameter between BG and POL cases.

Atmos. Chem. Phys. Discuss., https://doi.org/10.5194/acp-2017-806
Manuscript under review for journal Atmos. Chem. Phys.
Discussion started: 1 November 2017

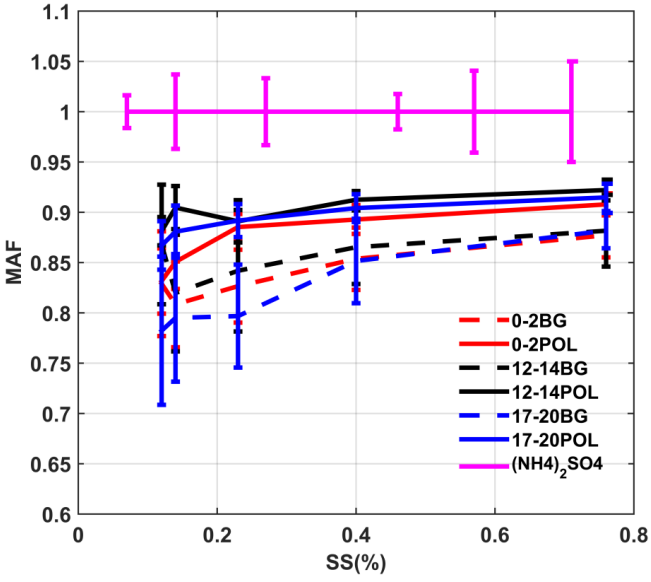

Figure 4. Mean maximum active fractions (MAFs) of CCN activation spectra under polluted (POL) and background (BG) conditions during the three periods, i.e., 0000–0200 LT, 1200–1400 LT, and 1700–2000 LT. The MAF of pure $(NH_4)_2SO_4$ particles at the different SS levels (magenta line) is also plotted.

Atmos. Chem. Phys. Discuss., https://doi.org/10.5194/acp-2017-806
Manuscript under review for journal Atmos. Chem. Phys.
Discussion started: 1 November 2017

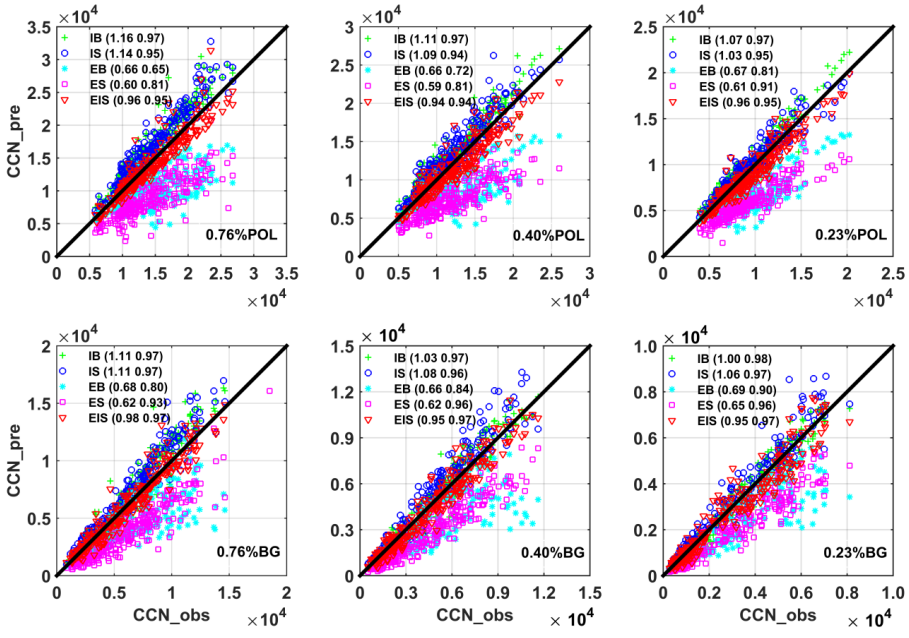

+ IB Internal mixture, bulk composition

o IS Internal mixture, size-resolved composition

*** EB External mixture, bulk composition**

□ ES External mixture, size-resolved composition

▽ EIS External mixture, POA and BC external mixed, size-resolved composition

Figure 5. Predicted N_{CCN} as a function of measured N_{CCN} using the five assumptions (colored symbols) at three supersaturation levels (0.23, 0.40, and 0.76%) under polluted (POL) and background (BG) conditions. The numbers in parentheses are the slope (first number) and the correlation coefficient (second number).

Atmos. Chem. Phys. Discuss., https://doi.org/10.5194/acp-2017-806
Manuscript under review for journal Atmos. Chem. Phys.
Discussion started: 1 November 2017

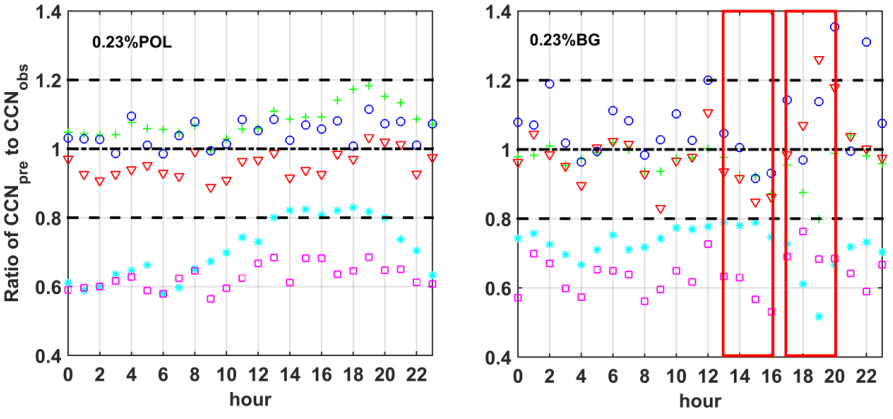

769

770 **+ IB Internal mixture, bulk composition**

771 **o IS Internal mixture, size-resolved composition**

772 *** EB External mixture, bulk composition**

773 **□ ES External mixture, size-resolved composition**

774 **▽ EIS External mixture, POA and BC external mixed, size-resolved composition**

775 **Figure 6.** Diurnal variations in the ratio of predicted-to-measured N_{CCN} at a
776 supersaturation level of 0.23% under background (BG) and polluted (POL)
777 conditions.

778

Atmos. Chem. Phys. Discuss., https://doi.org/10.5194/acp-2017-806
Manuscript under review for journal Atmos. Chem. Phys.
Discussion started: 1 November 2017

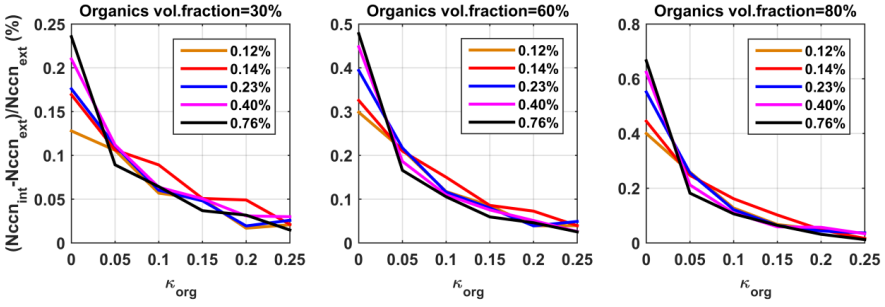

Figure 7. Relative deviations between N_{CCN} predicted under the assumptions of internal (IB) and external (EB) mixtures [(N_{CCN}.IB - N_{CCN}.EB) (N_{CCN}.EB)$^{-1}$] as a function of κ_{org} at organic volume fractions of 30, 60, and 80%. The solid lines with different colors represent different supersaturation levels (0.12, 0.14, 0.23, 0.40, and 0.76%).